Type-2 Fuzzy Logic Algorithm Based High Gain Improved Luo Converter for EV Applications

Conference Paper · August 2023

DOI: 10.1109/ICCPCT58313.2023.10245756

6 authors, including:

B. Kavya Santhoshi
Godavari Institute of Engineering and Technology (A)
24 PUBLICATIONS **141** CITATIONS
SEE PROFILE

R. Tharwin Kumar
Pondicherry Engineering College
30 PUBLICATIONS **34** CITATIONS
SEE PROFILE

Wisemin Lins
Vels University
7 PUBLICATIONS **17** CITATIONS
SEE PROFILE

2023 International Conference on Circuit Power and Computing Technologies (ICCPCT)

Type-2 Fuzzy Logic Algorithm Based High Gain Improved Luo Converter for EV Applications

B. Kavya Santhoshi
Assistant Professor,
Department of Electrical and Electronics Engineering, Godavari Institute of Engineering and Technology (A),
Rajahmundry, Andhra Pradesh, India.
kavyabe2018@yahoo.com

D. Lakshmi
Associate Professor,
Department of Electrical and Electronics Engineering,
AMET Deemed to be University,
Tamilnadu, India.
lakshmiee@gmail.com

R. Tharwin Kumar
Research Scholar,
Department of Electrical and Electronics Engineering, Puducherry Technological University,
Puducherry, India.
tharwin.eee@gmail.com

Sharda Patwa
Assistant professor
Department of Electrical engineering
Medi-caps University,
Indore, Madhyapradesh.
shardapatwa@gmail.com

A.Wisemin Lins
Assistant Professor
Department of Electrical and Electronics Engineering
Vels Institute of Science Technology and Advanced Studies
Tamilnadu, India
wisemin.se@velsuniv.ac.in

Murali Matcha
Associate professor
Department of Electrical Engineering,
Medicaps University,
Indore, Madhya Pradesh, India.
murali233.nitw@gmail.com

***Abstract*— The electrical grid's quality of power is compromised by the building of electric vehicle (EV) charging stations. This research suggests an electric vehicle period type 2 regulated high-quality charging system. For shunt conversion control, the fuzzy logic controller built on the immediately reactive power theory is suggested. The DC-link voltage measurement of the shunt converter's output and the entire harmonic distortion of the original present serve as the basis for assessment of type 1, interval type 2, and real programmed adaptive algorithm optimized fuzzy logic processors. These are also possible using the approach recommended by utilizing a high-end Power Quality bridgeless LUO conversion. The present Power Factor Correction (PFC) is constructed by coupling two separate, comparable half-cycle LUO converters with a conventional capacitor. Because typical PFC converter do not include input diode bridges, a converter offers a high density of power and low cost based EV charging technique with improved precision functioning in just one flipping cycle. The current from the input flows into a battery and the supply voltage is generated precisely on step, but the input power factor is high.**

Keywords*— EV-Electric Vehicle, FLC-Fuzzy Logic Controller, PWM-Pulse Width Modulation, MPPT-Maximum power Point Tracking, PI-Proportional Integral.

I. INTRODUCTION

Electric vehicles (EVs) are growing in popularity as a result of the scarcity of fossil fuels and environmental pollution, and electric vehicle charging stations have been proliferating swiftly in recent years. According to the Global Energy Agency's study "Global Electric Vehicle Outlook 2018," there were 4,054 charging stations in 2010 and 4,30,151 in 2017 [1]. In order to carry out the EVCS, various power electronic converters are used. Because of this, the transmission system experiences more issues, like instability in the voltage, harmonics, neutral current, power loss, etc. The researchers used a range of charger configurations and power levels to analyse the several problems with their network of distribution centres [2]. The different batteries architectural connections and charging power levels for plug-in and hybrid electric automobiles [3]. More harmonics are produced in the distribution system due to the EVCS's nonlinear power electronics converters. Numerous charger topologies, including single-phase unchecked rectifiers, bidirectional regulation rectifiers, three-phase uncontrolled rectifiers, thyristorized unregulated rectifiers. Both of and bidirectional controllable rectifiers, and are used to analyse harmonic [4]. A three-phase uncontrolled rectifier-based charger's supply current has an average distortion due to harmonics of 30%. A three-phase unidirectional converter-based chargers generated THD of 8.1% and 9.4% during grid to automotive and automobile to grid processes, correspondingly. On the other hand, the controls were built using a fuzzy logic approach. For smaller systems, a conventional or type 1 FLS is more effective [5]. When compared to their T1 equivalents, the IT2 FLC delivers cleaner control surfaces and is more dependable, according to the steady-state analysis [6]. The highly efficient non-linear diode bridge rectifier (HDD) utilized by the electric car charger only uses DC electricity at the converter's DC to DC inputs, addressing serious power quality issues at the current AC input. These issues required battery chargers to deliver substantially higher-quality power, which could be accomplished by removing their input bridges [7]. These are also achieved by incorporating a high-end Power Quality bridgeless LUO converter into the recommended method. The current PFC converter is actually an addition of two autonomous, comparable half-cycle LUO converters that make use of a common capacitors. Due to the lack of an input diode bridge in traditional PFC converters, a converter offers a high power density and low cost based EV charging technique with improved accuracy functioning in just one switch cycle [8]. The source voltage is created precisely on step in the case of a charger, and the input current changes, yet the input power factor is large. Currently, an EV charger is all that is required to modify a bridgeless LUO converter. Additionally accessible are the LUO conversion and the AC source. The BL PFC converter is created by combining the LUO PFC converter for switches S1, S2, and a common input inductor, L. Generators for high-frequency operation now have this conversion, which is utilized to boost the output at medium frequencies. Receiving is the transformer's output from the fly-back converter [9]. Use of a fly-back converter is required when using a single controlled switch that has a MOSFET. It has the ability to charge and discharge batteries.

979-8-3503-3324-4/23/$31.00 ©2023 IEEE

The single controller used in this architecture is the pic16f877a. The opto controller unit has provided PWM signal converter switching using the control unit. The LUO converter, the controller, and the voltage measurement instrument send measurements of voltage and current to the regulators on a regular basis [10]. As a result, they have become a major cause for concern in the MPPT about long-term structures. To monitor the output power of the PEMFC system, a new type-1 fuzzy logic-based adjustable step size MPPT control system has been developed. The results were contrasted to demonstrate the edge of their suggested controller, and the fuzzy logic method was also employed to modify the IC MPPT microcontroller's customizable step size [11]. The outcomes demonstrated that fuzzy logic may be employed for controlling fuel cell systems' dynamic behavior. Similar to this, a novel hybrid MPPT solution is based on the combination of type-1 fuzzy logic technology and the parameter perturbation-current step approach for frigid temperatures [12]. To operate the fuel systems at lower temperatures, a temperature controller stage was also built. These methods, however, have a number of flaws that prevent them from being easily used to aggregate and produce decision-making components (such membership functions (MFs) and rules [13]. The MPPT strategy, which will be employed for fuel cell devices, has instead been the subject of development [14]. The major goal of this study is to design and construct a unique self-tuning MPPT controller for PEMFC electric vehicles in order to deliver energy with the lowest cost, highest efficacy, and best provider reliability possible [15].

- To improve output from EV system using Improved Luo converter.
- To tracking maximum power point from EV using Type-2 Fuzzy.
- To provide grid and synchronization using PI controller.

II. Proposed Syste Description

The High Gain improved Luo converter based type 2 fuzzy MPPT showed in Fig. 1.

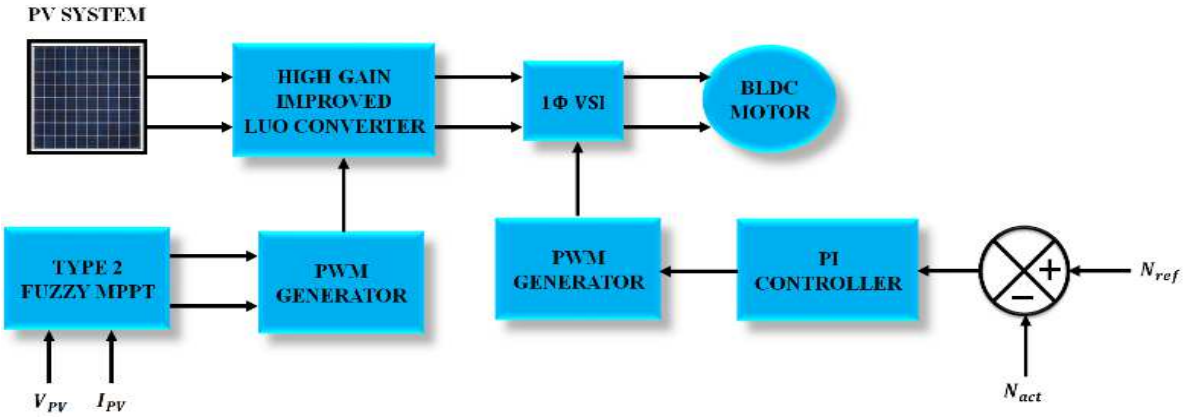

Fig. 1. Proposed Block Diagram

Due to the fluctuating climatic circumstances, tracking the module's maximum power point EV systems is difficult. To the Improved Luo converters, the inner tracking ray is transmitted. A converter output voltage is increased and kept consistent through the system using the suggested Improved Luo converter. The PI controller generates the actual and reference power to the PWM generator and it transfers the output to the Voltage source Inverter. The recommended MPPT technique and the EV classification were together replicated consuming the Mat lab/Simulink.

III. Proposed System Modelling

A. PV System

The PV system utilized for power adaptability is made up of various sequences and equivalent combinations of PV modules, a subsequent supervisor, and power converters such a DC-DC converter and inverter. As a result, a DC to DC converter can be used to increase the DC voltage generated, and an inverter can be used to convert the DC energy to AC. It is important to confirm that the PV panel is original to its weight rating.

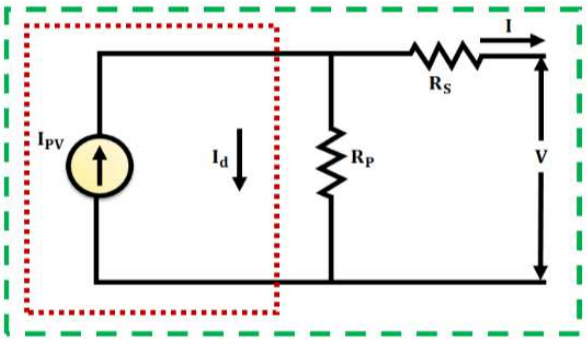

Fig. 2. Corresponding circuit of PV cell

The diode Shunt resistanceR_{sh}, Series ResistanceR_s. Shunt ResistanceR_{sh}.

$$I = I_{ph} - I_d - I_{sh} \quad (1)$$

$$I_d = I_0 \left\{ \exp\left[\frac{q}{mkT_c}(V + IR_s)\right] - 1 \right\} \quad (2)$$

$$I_{sh} = \frac{V+IR_s}{R_{sh}} \quad (3)$$

By applying Calculations is shown below

$$I = I_G - I_0 \left\{ exp\left[\frac{q}{mkT_c}(V + IR_s)\right] - 1 \right\} - \frac{V+IR_s}{R_{sh}} \quad (4)$$

Typically shunt Resistance R_{sh} in PV cells is high hence $\frac{V+IR_S}{R_{sh}}$ is removed

$$I = I_G - I_0\left\{exp\left[\frac{V+IR_S}{A}\right] - 1\right\} \quad (5)$$

Where A=curve fitting restriction

$$A = \frac{mkT_c}{q} \quad (6)$$

According to Fig. 2 output current at normal trial circumstance is

$$I = I_{ph} - I_0\left[exp\left(\frac{V}{a}\right) - 1\right] \quad (7)$$

After PV cell is dumpy circuited

$$I_{sc} = I_{ph} - I_0\left[exp\left(\frac{0}{a}\right) - 1\right] = I_{ph} \quad (8)$$

$$I_{ph} \approx I_{sc} \quad (9)$$

The photocurrent rest on composed irradiance and temperature

$$I_{ph} = \frac{G}{G_{ref}}\left(I_{ph} + \mu_{sc}.\Delta T\right) \quad (10)$$

G=irradiance

G_{ref}=irradiance at standard testing conditions

The voltage (V_{mp}) and current (I_{mp}) at maximum power is

$$I_{sc} = I_{ph} - I_0\left[exp\left(\frac{I_{sc}.R_S}{A}\right) - 1\right] \quad (11)$$

$$O = I_{ph} - I_0\left[exp\left(\frac{V_{oc}}{A}\right) - 1\right] \quad (12)$$

$$I_{pm} = I_{ph} - I_0\left[exp\left(\frac{V_{pm}+I_{pm}R_S}{A}\right) - 1\right] \quad (13)$$

According to Equation (10) substituting (I_{ph}) in Equation (13)

$$0 \approx I_{sc} - I_0 exp\left(\frac{V_0}{A}\right) \quad (14)$$

Hence,

$$I_0 = I_{sc}\, exp\left(\frac{-V_{0c}}{A}\right) \quad (15)$$

B. PWM Generator

The pulse width message signal is created by the PWM generator and applied to the inverter's switches. The PWM generator actually divides the average power reduction into distinct portions. Due to this extended ON time, more electricity will be provided. Pulse width modulated gate pulse signals are primarily produced by the Generator and then supplied to the switching inside the converter. Using a two-level design, the PWM Generating block produces beats for carrier-based PWM conversions. On separate, multiple, thirty compelled machinery can be generated by the block (FETs, GTOs, or IGBTs).

C. PI Controller

PI controller integral of that value and a weighted total of errors are used to operate the plant that has to be regulated. Almost every process presently in use, from control of motion to aviation, and from sluggish to fast structures, has been controlled by PI-Controllers. Due to modifications to system behavior and variations in operation scores, PI-Controllers must also be retrieved frequently. As a result, numerous research have focused on the potential and options of the referred to as adaptable PI controllers.

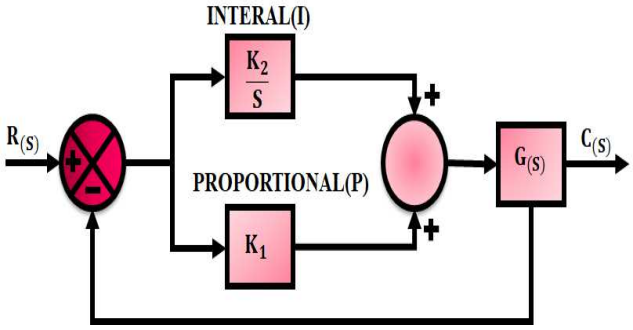

Fig. 3. Basic Block of PI Controller

The Controller increases both the system's order and type by one. Additionally, compared to proportionate alone control, it results in a steady state error reduction to zero. The PI controller increases fluctuation and decreases intensity. Furthermore, it increases rising time while reducing frequency. Derivatives activity may increase the system's steady-state stability in the situation of noisy data. This is due to the higher influence of the frequently occurring terms in the input data on the derivative activity. The PI controlled system is less responsive to genuine (non-noise) in the lack of action from derivatives.

D. High Gain Improved Luo Converter

To improve the output from the PV system the high gain Luo converter is employed. Fig. 4 depicts the Buck-output Luo converter's electronics layout. Magnets are the inert elements which hold power.

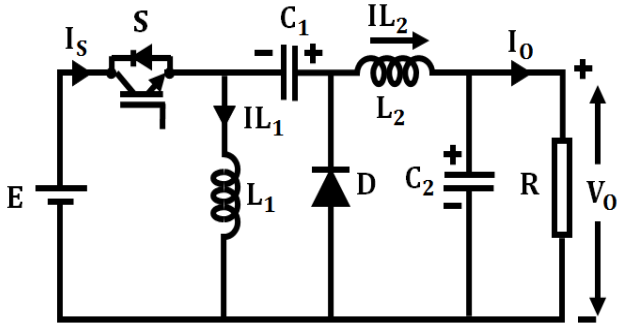

Fig. 4. Path figure of Luo converter

Utilized are resistors L1, L2, and capacitance C1, C2, with R standing for the load admittance. The structure can be split into two different states to find out how the Luo converter works. The source of voltage E compresses the conductor L1 when a switch is ON. Energy from the source is simultaneously absorbed by the inductor L2 and its capacitor C1. Power for the load is provided by Concentrator C2. The comparable Luo conversion circuit is shown in (a) functioning in mode 1. As seen in (b), no electrical current is drawn from the source while the switch is in the OFF position. The resultant voltage's harmonics levels will

decrease if additional filter components, like a resistor and a capacitor that stores electricity, are added.

Modes of Operation

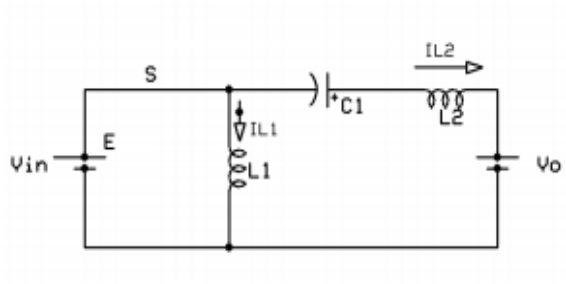

(a)

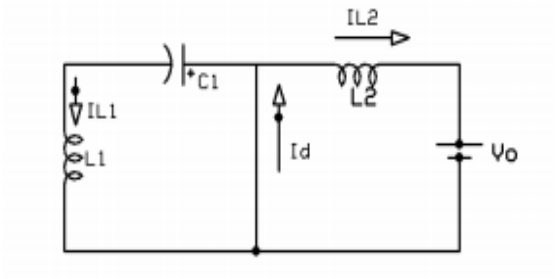

(b)

Fig. 5. Model of Operation

The output in the mode of discontinuous conduction should take the form of a discontinuity. The inductor discharges through V0 and L2 in this mode since there is no diode.

The inductor current IL_2,

$$IL_2 = \frac{1-a}{a} IL_1 \tag{16}$$

Duty cycle,

$$\mathrm{a} = \frac{T_{on}}{T} \tag{17}$$

Production power calculation,

$$V_0 = \frac{a}{1-a} V_{in} \tag{18}$$

Regular Power crossways the capacitor C1 is,

$$V_{c1} = \frac{a}{1-a} V_{in} \tag{19}$$

Peak to peak inductor present is,

$$VT_{L1} = \frac{aTV_{in}}{L_1} \tag{20}$$

Equation (20) inductor L1 value,

$$`L_1 = \frac{aTV_{in}}{\nabla IL_1} \tag{21}$$

Peak to peak inductor existing L2 is,

$$\nabla_{I_{L2}} = \frac{aTV_{in}}{L_2} \tag{22}$$

Calculation (21) inductor L2 worth,

$$L_2 = \frac{aTV_{in}}{\nabla_{I_{L2}}} \tag{23}$$

The current on the parallel capacitance (C1) rises by IL2 (=Io) throughout the off time and falls by IL1 throughout the on period. Peak to peak ripple voltages across a capacitor like C1 must not modify the amount of charge on C1.

$$\nabla V_{c1} = \frac{1-a}{C_1} TI_1 \tag{24}$$

Equation (24) C1 value,

$$C_1 = \frac{1-a}{\nabla V_{c1}} TI_2 \tag{25}$$

E. Type 2 Fuzzy MPPT

To track the maximum power from the EV application the fuzzy logic theory is used. Physical contrast of the environment and the system under consideration impose two fundamental circumstances: the attendance of indecision in the structure and fleeting reply of the organization. This is because the interferences might be more properly modelled and considered by fuzzy type-2. Interference or the presence of noise. The fuzzy logic as a viable solution for reducing the consequences of uncertainty. However, if adaptive accessories are added to the designed fuzzy controller, the entire system becomes incredibly effective at estimating unknown functions. Uncertainties and interferences are significant obstacles when trying to develop a reliable or robust controller due to unknown system components. The type-2 one is one of the common and efficient fuzzy family controllers.

The use of a fuzzy controller ensures MPPT. A DC-DC converter is castoff to maintain the PV terminal voltage at the point where the most power is absorbed as well as to competition the production power of the PV gathering with the essential load voltage. The preparation of the adapting mechanisms of the DC to DC convertor is managed by the FLC controller. Equation for a DC-DC converter's input-output:

$$\mathrm{V_{PV}} = \mathrm{V_0}(1 - \mathrm{D}) \tag{26}$$

V0 and D are the production voltage and the cycle of a DDC converter, respectively, where Vpv is the PV voltage.

In order to accommodate greater uncertainty, the fuzzy controller type-2 organization sweeping the fuzzy controller type-1 system. As a result, the type-2 fuzzy controller has been employed in this project. Fitting a single membership function to a single state continuously may not work in this type. Therefore, it is conceivable to anticipate improved and more truthful presentation of the organization in the case of uncertainty as long as we define membership functions unquestionably.

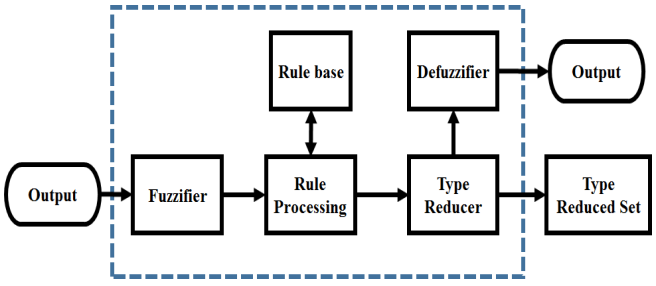

Fig. 6. Type 2 fuzzy logic controller

IV. Results And Discussion

Millions of scientists and technologists employ the great equal linguistic and collaborating setting known as MATLAB. In these schemes, the proposed Improved Luo converter is coupled to the EV module to enable the maximum output voltage under any given circumstance. A novel approach of tracking the greatest influence opinion in the presence of multiple local maxima called Type-2 Fuzzy MPPT has been included in the suggested system. Table 2 represents the parameters specification.

TABLE 1. Parameter Specification

Specifications	Values
Inductances (L_1, L_2)	$4mH, 6mH$
Capacitances (C_1, C_2)	$220\mu F, 100\mu F$
Switching Frequency (f_s)	$25KHz$
Resistive Load (R_L)	15Ω

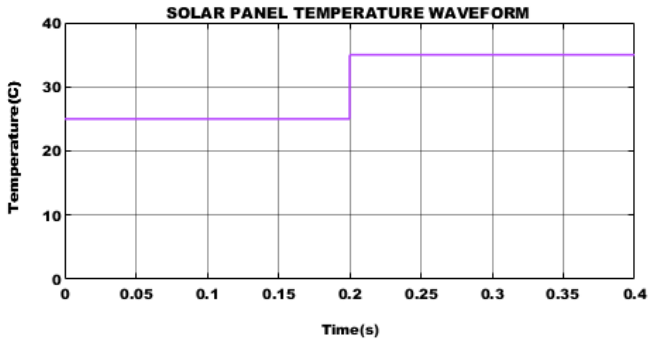

Fig. 7. Solar panel temperature waveform

Fig. 7 indicates the waveform for Solar panel Temperature and it represents a constant DC voltage. The Temperature is maintains at 25C up to the time period of 0.2s. After 0.2s the temperature increasing to 35C and further it is maintains constant.

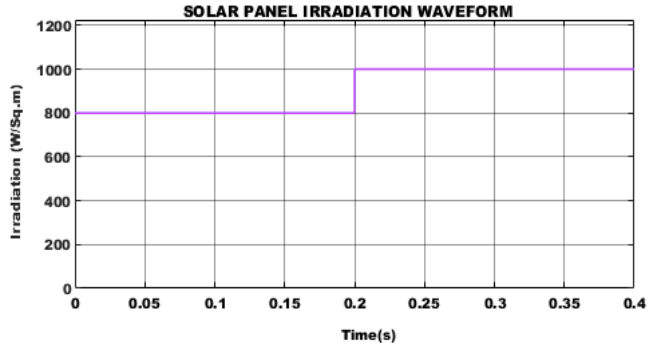

Fig. 8. Solar panel irradiation waveform

The Solar panel Irradiation Waveform maintains at 800W/Sq-m up to the time period of 0.2s as shown in Fig. 8. After 0.2s the solar panel irradiation waveform increasing to 1000W/Sq-m and further it is maintains constant.

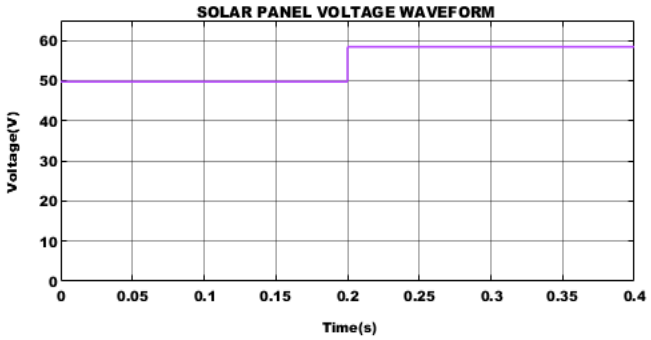

Fig. 9. Solar panel voltage waveform

The solar panel voltage waveform is maintains at 50V up to the time period of 0.2s as shown in Fig. 9. After 0.2s the solar panel voltage waveform increasing to 59V and further it is maintains constant.

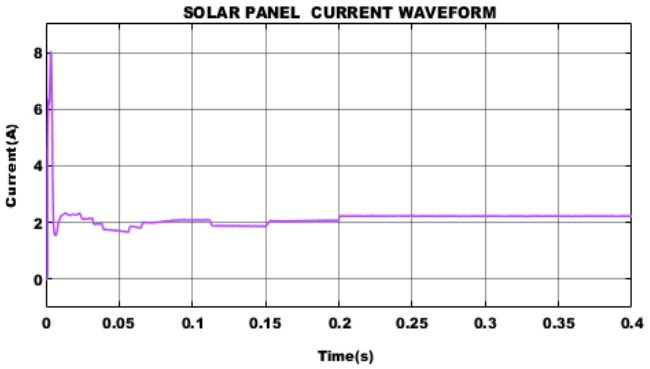

Fig. 10. Solar panel current waveform

Fig. 10 indicates the solar panel current waveform is maintains at 2A up to the time period of 0.03s. After 0.03s the output power increasing to 8A and further it is maintains constant.

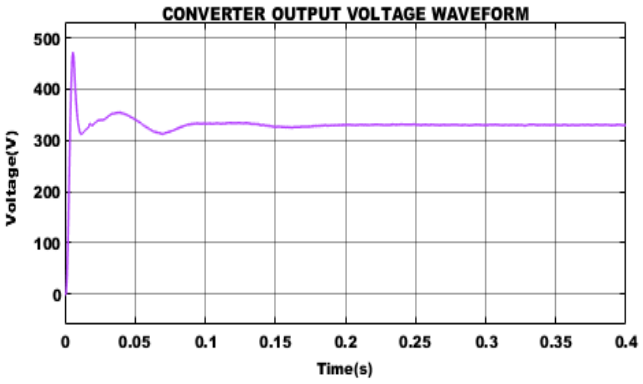

Fig. 11. Converter output voltage waveform

Fig. 11 indicates the converter output voltage waveform for output power is maintains at 450V up to the time period of 0.03s. After 0.03s the output power decreasing to 300V and further it is maintains constant.

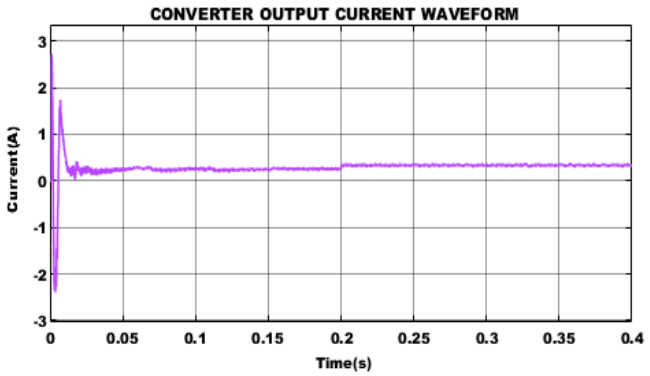

Fig. 12. Converter output current waveform

Fig. 12 indicates the converter output current waveform slightly increases up to the time period of 0.01s. After 0.01s the waveform decreased up to the time period of 0.03s and further it is maintain constant.

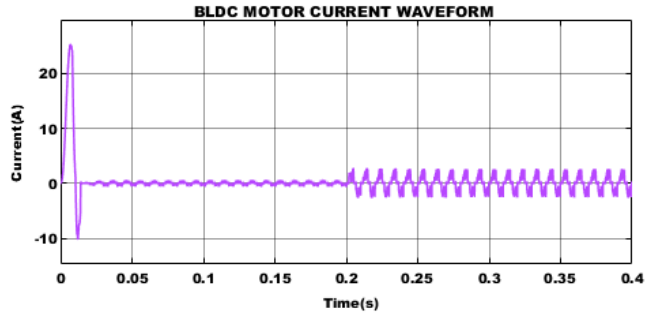

Fig. 13. BLDC motor current waveform

Fig. 13 indicates the BLDC motor current waveform slightly increases up to the time period of 0.01s. After 0.01s the waveform decreased up to the time period of 0.03s and further it is maintain constant.

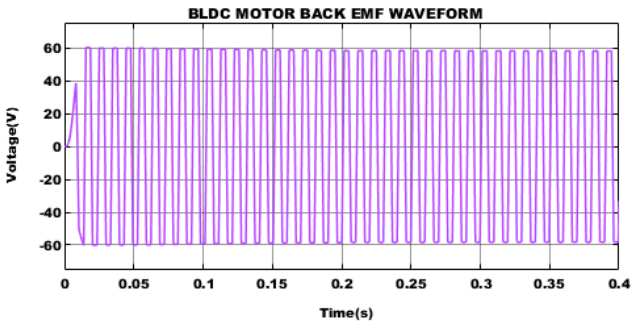

Fig. 14. BLDC motor back EMF waveform

The output of the BLDC Motor back EMF waveform achieves a constant voltage of 60V as shown in Fig. 14.

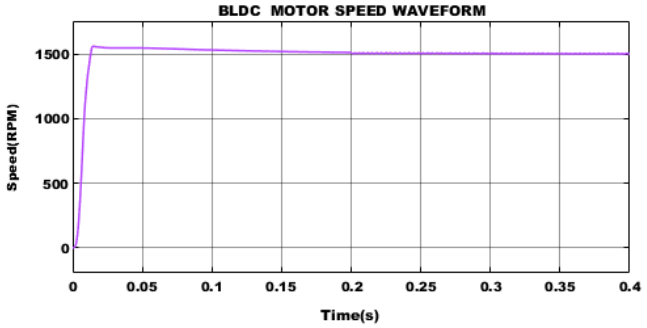

Fig. 15. BLDC motor speed waveform

Fig. 15 indicates the BLDC motor speed waveform increases 1600RPM up to the time period of 0.02s and further it is maintain constant.

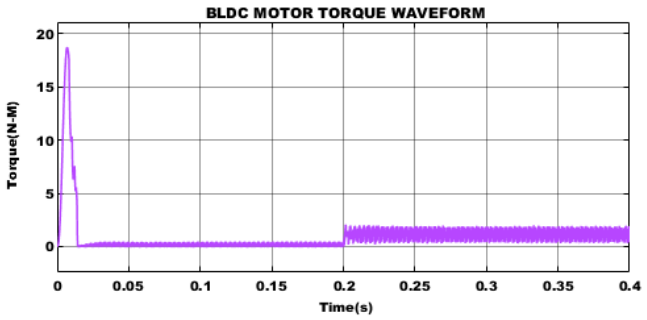

Fig. 16. BLDC motor torque waveform

Fig. 16 indicates the BLDC motor torque waveform increases 19N-M up to the time period of 0.02s, after 0.02s the waveform decreases and further it is maintain constant.

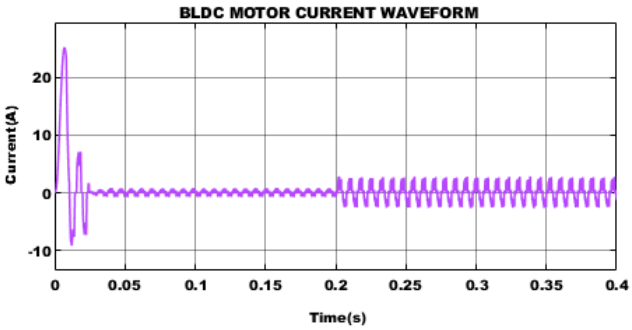

Fig. 17. BLDC motor current waveform

Fig. 17 indicates the BLDC Motor current waveform slightly increases up to the time period of 0.01s. After 0.01s the waveform decreased up to the time period of 0.03s. After 0.03s the waveform increases and further it is maintain constant.

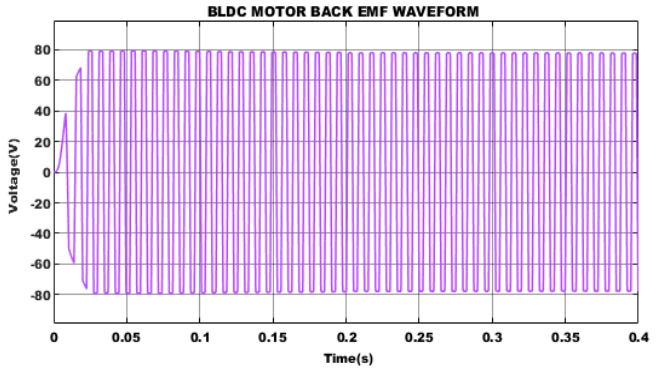

Fig. 18. BLDC motor back EMF waveform

The output of the BLDC Motor back EMF waveform achieves a constant voltage of 80V as shown in Fig. 18.

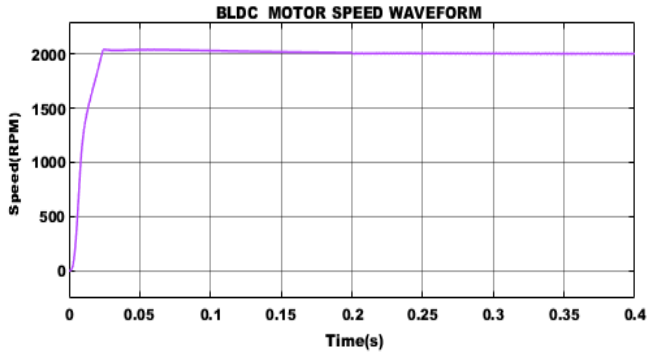

Fig. 19. BLDC motor speed waveform

Fig. 19 indicates the waveform BLDC Motor speed waveform is maintains at 100RPM. After 0.02s the waveform increasing to 2000RPM and further it is maintains constant.

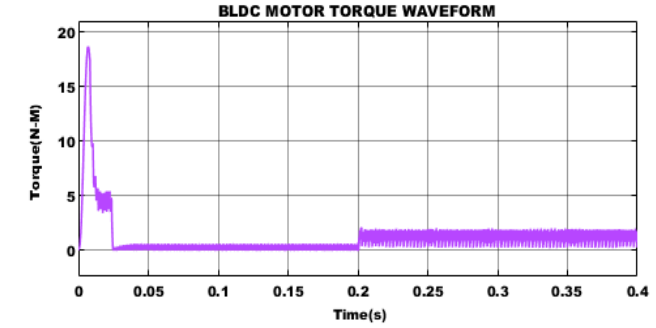

Fig. 20. BLDC motor torque waveform

Fig. 20 indicates the BLDC motor torque waveform increases 19N-M up to the time period of 0.02s, after 0.02s the waveform decreases and further it is maintain constant.

The comparison of the THD values of the converters are listed in Fig. 21, in which they are listed as 5.14%, 4.1%, 3, 29% and 2.1% Cuk, Sepic, and Luo and improved luo respectively. The proposed attain low THD value than the conventional approaches.

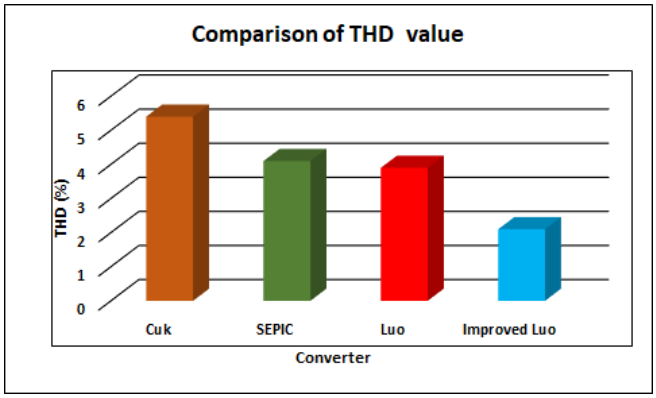

Fig. 21. THD Value Comparison

V. Conclusion

In EV systems, it is challenging to monitor the MPPT of the module because of the constantly changing environmental conditions. The tracking method also becomes more challenging due to the several peaks in the power voltage characteristics under partial shade. A consistent power from the EV at the required voltage level is achieved with the aid of a Type 2 fuzzy MPPT and a very effective improved Luo conversion. The PV panel's output is always maximized via the Type 2 fuzzy technique. The type 2 fuzzy-based MPPT controller works effectively and yields superior outcomes. The MATLAB simulation results show that the suggested method is successful in maintaining the dependability and stability of the output voltage system in partially shaded settings.

References

[1] S. M. Shyni, and R. Ramadevi, "Design of fuzzy logic controller for fused Luo converter based solar/wind hybrid green energy system," Environment, Development and Sustainability, pp. 1-24, 2021.

[2] P. Bayat, and A. Baghramian, "A novel self-tuning type-2 fuzzy maximum power point tracking technique for efficiency enhancement of fuel cell based battery chargers," International Journal of Hydrogen Energy, vol. 45, no. 43, pp. 23275-23293, 2020.

[3] G. Luo, B. Ma, Z. Wang, L. Yin, and Y. Wang, "Model-free adaptive control for the PEMFC air supply system based on interval type-2 fuzzy logic systems," Journal of Renewable and Sustainable Energy, vol. 12, no. 6, pp. 064301, 2020.

[4] I. Benlaloui, L. Chrifi-Alaoui, M. Ouriagli, A. Khemis, D. Khamari, and S. Drid, "Improvement of the induction motor sensorless control based on the type-2 fuzzy logic," Electrical Engineering, vol. 103, no. 3, pp. 1473-1482, 2021.

[5] S. Venkatesan, M. Saravanan, and S. Venkatanarayanan, "Signal-flow graph analysis and implementation of novel power tracking algorithm using fuzzy logic controller," International Journal of Business Intelligence and Data Mining, vol. 18, no. 1, pp. 88-108, 2021.

[6] C. Balasundar, C. K. Sundarabalan, N. S. Srinath, and J. M. Guerrero, "Interval type-II fuzzy logic controlled shunt converter coupled novel high-quality charging scheme for electric vehicles," IEEE Trans. Ind. Informat, 2020.

[7] Y. Cao, A. Mohammadzadeh, J. Tavoosi, S. Mobayen, R. Safdar, and A. Fekih, "A new predictive energy management system: Deep learned type-2 fuzzy system based on singular value decommission," Energy Reports, vol. 8, pp. 722-734, 2022.

[8] S. Cantillo-Luna, R. Moreno-Chuquen, F. Gonzalez-Longatt, and H. R. Chamorro, "A Type-2 Fuzzy Controller to Enable the EFR Service from a Battery Energy Storage System," Energies, vol. 15, no. 7, pp. 2389, 2022.

[9] S. Paul, R. Turnbull, D. Khodadad, and M. Löfstrand, "A Vibration Based Automatic Fault Detection Scheme for Drilling Process Using Type-2 Fuzzy Logic," Algorithm, vol. 15, no. 8, pp. 284, 2022.

[10] R. Rodriguez, J. P. F. Trovão, and J. Solano, "Fuzzy logic-model predictive control energy management strategy for a dual-mode locomotive," Energy Conversion and Management, vol. 253, pp. 115111, 2022.

[11] P. C. Sahu, S. Mishra, R. Chandra Prusty, and S. Panda, "Improved-salp swarm optimized type-II fuzzy controller in load frequency control of multi area islanded AC microgrid," Sustainable Energy, Grids and Networks, vol. 16, pp. 380-392, 2018.

[12] N. Priyadarshi, M. S. Bhaskar, F. Azam, M. Singh, D. K. Dhaked, I. B. M. Taha, and M. G. Hussien, "Performance evaluation of solar-PV-based non-isolated switched-inductor and switched-capacitor high-step-up cuk converter," Electronics, vol. 11, no. 9, pp. 1381, 2022.

[13] S. Cantillo-Luna, R. Moreno-Chuquen, F. Gonzalez-Longatt, and H. R. Chamorro, "A Type-2 Fuzzy Controller to Enable the EFR Service from a Battery Energy Storage System", Energies, vol. 15, pp. 2389.

[14] W. J. Chang, Y. W. Lin, Y. H. Lin, C. L. Pen, and M. H. Tsai, "Actuator saturated fuzzy controller design for interval type-2 Takagi-Sugeno fuzzy models with multiplicative noises," Processes, vol. 9, no. 5, pp. 823, 2021.

[15] C. Küçükkeçeci, "Multilevel object tracking on big graph data using interval type-2 fuzzy systems in wireless multimedia sensor networks," 2020.